RSC Advances

PAPER

Cite this: *RSC Adv.*, 2020, **10**, 6200

Biofunctionalization of zirconia with cell-adhesion peptides *via* polydopamine crosslinking for soft tissue engineering: effects on the biological behaviors of human gingival fibroblasts and oral bacteria†

Zhen Yang,‡[a] Mingyue Liu,‡[b] Yang Yang,[a] Miao Zheng,[c] Yang Yang,[a] Xiaoqiang Liu[a] and Jianguo Tan*[a]

Rapid soft tissue integration is essential for long-term dental implant success. Zirconia is increasingly used as an abutment material owing to its excellent aesthetic properties and biocompatibility; however, it is bioinert, and tissue integration is poor. We developed a feasible surface modification method, exploiting the reactivity of polydopamine (PDA) films to immobilize cell-adhesion peptides (Arg-Gly-Asp, RGD) onto zirconia abutment surfaces. Further, we evaluated the effect thereof on human gingival fibroblast (HGF) behavior and oral bacterial adhesion, which influence the peri-implant soft tissue seal. HGF responses to linear KGGRGDSP and cyclic RGDfK sequences were compared. PDA deposition and covalent coupling of RGD were verified by X-ray photoelectron spectroscopy and fluorescence microscopy. The biological behaviors of HGFs on the modified zirconia; *i.e.*, adhesion, spreading, proliferation, gene and protein expression, were elucidated. Biofunctionalization of zirconia with the adhesion peptides significantly enhanced the biological activities of HGFs. Cyclic RGD induced slightly improved cell attachment, spreading, and proliferation, but similar cell differentiation when compared to linear RGD peptides. To assess their antimicrobial properties, the different substrates were exposed to cultures of the early colonizer *Streptococcus mutans* or the periodontal pathogen *Porphyromonas gingivalis*, and bacterial adhesion was evaluated by scanning electron microscopy and live/dead staining. PDA and PDA-RGD coatings decreased zirconia surface colonization by both bacterial species to similar extents. Thus, PDA-RGD-functionalized zirconia modulates specific HGF responses, while maintaining the antimicrobial activity of the PDA coating. The selective bio-interaction pattern of this surface modification holds great promise for improving soft-tissue integration around zirconia abutments in clinical applications.

Received 20th October 2019
Accepted 9th January 2020

DOI: 10.1039/c9ra08575k

rsc.li/rsc-advances

1. Introduction

Dental implants are extensively used to replace missing teeth.[1] Long-term implant stability relies not only on successful osseointegration but also on effective integration of the implant surface with the surrounding soft tissue. The soft tissue seal around the implant abutment acts as a barrier between the oral environment and the alveolar bone, thus preventing bacterial penetration, protecting the underlying bone, and maintaining the normal shape of the gingiva.[2] However, soft tissue around the implant abutment is different from that around natural teeth; it has fewer human gingival fibroblasts (HGFs), lacks vascularity, and peripheral fibers are arranged in parallel, leading to relatively poor bacterial resistance and ultimately influencing restoration longevity.[3] This limitation can be overcome, in part, by modifying the implant surfaces to allow better adhesion to the soft tissue. Accordingly, the improvement in soft tissue compatibility *via* implant surface modification has become a research focus.

The soft tissue seal surrounding dental implants can be affected by microbial infection. Early infections usually originate from microbial contamination during and immediately

[a]*Department of Prosthodontics, Peking University School and Hospital of Stomatology, National Clinical Research Center for Oral Diseases, National Engineering Laboratory for Digital and Material Technology of Stomatology, Beijing Key Laboratory of Digital Stomatology, Beijing, 100081, P. R. China. E-mail: tanwume@vip.sina.com; Fax: +86-10-62173402; Tel: +86-10-82195364*

[b]*First Clinical Division, Peking University School and Hospital of Stomatology, Beijing, 100034, P. R. China*

[c]*Department of Stomatology, Peking University Third Hospital, Beijing, 100191, P. R. China*

† Electronic supplementary information (ESI) available. See DOI: 10.1039/c9ra08575k

‡ These authors contributed equally to this work.

after surgery. Contaminating pathogens, including early colonizers such as streptococci, and host cells such as fibroblasts compete to cover the implant, which was described as "race for the surface" by Gristina *et al.*[4] If bacteria occupy the surface before host cells arrive, a plaque biofilm will be formed that protects the bacteria from being replaced by tissue cells, thus influencing soft tissue barrier formation. Late infections (peri-implantitis/peri-implant mucositis) present a different form of race for the surface, *i.e.*, peri-implantitis pathogens displace periodontal ligament fibroblasts from the implant surface, leading to adjacent tissue damage or even implant failure.[5] Indeed, peri-implant lesions are among the most frequent and severe implant complications, and are difficult to treat.[6] In this regard, early formation of an effective and durable soft tissue seal is important from the prophylaxis point of view. Host and bacterial cell attachment is directly affected by specific material surface characteristics, such as topography and roughness, wettability, electrical charge, and chemical composition.[7,8] Thus, to improve soft tissue reactivity, surface modification of the implant material should provide a biological interface that facilitates host cell integration while minimizing bacterial adhesion.

The use of zirconia as implant abutment material is rapidly increasing, since it is regarded as being more aesthetic and biologically friendly compared with traditional abutment material, titanium.[9] However, because it is bioinert and has low reactivity, the use of zirconia is challenging when it comes to fast integration with the surrounding tissue.[10] To address this issue, several surface modification approaches have been proposed to improve the biological performance of zirconia in terms of tissue responses: (i) modifying the surface topography by grinding, sand blasting,[11] or etching;[12] (ii) application of ultraviolet irradiation,[13] plasma spraying,[14] or laser treatment;[15] and (iii) coating of the surface with bioactive agents such as hydroxyapatite,[16] calcium phosphate,[17] chitosan,[18] type I collagen,[19] and bone morphogenetic protein 2.[20] Among these techniques, the physical methods require specialized equipment and conditions, while bioactive coatings generally require complicated procedures and frequently demonstrate poor adhesion to the material. Moreover, the major purpose of these surface modification strategies is to promote bone regeneration, while data on their effect on soft tissue healing are lacking. Therefore, there is an urgent need for a simple and effective surface treatment method to improve the bioactivity of zirconia with regard to soft tissue integration.

Functionalization of dental implant surfaces using biomimetic agents is a hot topic in the biological materials research field.[10,21] The presence of biomolecules on the surface of biomaterials mimics the native cellular microenvironment in dictate of cell behavior. For example, Arg-Gly-Asp (RGD), a cell-binding sequence derived from the extracellular matrix (ECM) protein such as fibronectin, has been extensively employed because it promotes cell adhesion by activating integrin receptors. RGD-containing peptides enhance the attachment of numerous cell types on various types of biomaterials.[22] The anchoring of RGD to the substrate determines tissue integration. RGD peptides that detach from the substrate may inhibit cell adhesion by competing with attached RGD for integrin on target cells.[21] Therefore, efficient immobilization of the RGD peptide is a major concern in the preparation of cell adhesion-promoting surfaces. Various immobilization methods have been developed to tether RGD peptides onto dental implant surfaces, including electrodeposition,[23] plasma polymerization,[24] self-assembled monolayers,[25] and covalent coupling.[26] However, many of these strategies have limitations, such as low binding stability, low grafting rate, complex chemical processes, use of organic solvents, and being time-consuming and/or costly.[27] In addition, RGD peptides have been extensively used to coat titanium implants,[28–30] but rarely for zirconia abutments. Moreover, little is known about the antimicrobial properties of RGD coating. Thus, a facile, efficient, and low-cost immobilization method to stably graft RGD peptides onto zirconia surfaces would be highly beneficial.

Inspired by the bio-adhesion principle of mussels, Messersmith *et al.* developed a versatile polydopamine (PDA) coating by simply dipping the substrate into an alkaline dopamine solution. The PDA film formed strong adhesive interactions with diverse materials, regardless of their chemistry or geometry.[31] More importantly, PDA coating facilitates covalent conjugation with biomolecules containing amine and thiol groups *via* Michael addition or Schiff base reactions, which enables the preparation of various hybrid materials with specific functionalities. Various proteins, peptides, and bioactive molecules have been conjugated onto substrates *via* the PDA coating layer for different purposes.[32,33] Previous data from our group demonstrated that PDA is able to modify zirconia surfaces and improve the adherence of HGFs to a certain extent. Moreover, PDA coating also possesses favorable antibacterial properties.[34] However, PDA coating alone did not sufficiently promote biological behaviors of HGFs. To further improve the specificity of zirconia abutment materials and cell–surface interactions, in the current study, cell adhesion peptides containing RGD sequences were immobilized onto zirconia surfaces *via* the PDA coating layer. Compared to traditional immobilization approaches, PDA-assisted surface modification exhibits several advantages as (1) it significantly improves the anchoring of biomolecules; (2) it is a simple method that does not require time-consuming synthesis of complex linkers; (3) the process is non-toxic and uses water as a solvent, reducing the risk of damaging the biological activity of the adhesion molecules; and (4) it can be applied to complex geometries.[35] Chien *et al.*[36,37] reported that implant surface functionalization with RGD-conjugated polymers *via* PDA-assisted immobilization promoted titanium biocompatibility and osteogenic response. However, to the best of our knowledge, the effect of PDA-assisted RGD peptide grafting on soft tissue healing around zirconia abutment surfaces has not yet been explored.

We aimed to develop a facile and effective coating method based on PDA deposition for immobilizing cell-adhesion RGD peptides on zirconia abutment materials to improve soft tissue integration. The effect of peptide-based biomimetic functionalization on bioactivity was assessed using two different types of ligand, *i.e.*, a linear (KGGRGDSP) and a cyclic (c(RGDfK)) RGD peptide. To evaluate the coating efficacy, the biological behavior

of HGF such as adhesion, spreading, proliferation, and differentiation as well as gene and protein expression were investigated *in vitro*. Moreover, the effect of immobilized RGD peptide on bacterial adhesion was also studied (Scheme 1).

2. Materials and methods

2.1. Materials

Zirconia disks (Zenostar, Wieland Dental, Pforzheim, Germany) were cut to 15 mm in diameter and 2 mm thick using a cutting machine. The disks were wet-grinded and serially polished with 600-, 800-, and 1200-grit SIC abrasive papers. The crystallographic structure of zirconia was analyzed as reported previously,[34] and the results showed that it fitted the properties of zirconium yttrium oxide. All disks were washed in an ultrasonic cleaner in absolute ethanol and distilled water for 20 min each, and then dried in an oven at 50 °C before surface treatment.

2.2. Preparation of substrates

PDA coating was performed as described previously.[31] Briefly, disks were immersed in dopamine solution (2 mg mL^{-1} in 10 mM Tris–HCl, pH 8.5, Sigma-Aldrich, St. Louis, MO, USA) and gently shaken at room temperature for 18 h. The PDA-coated disks were extensively rinsed with copious ultrapure water to remove unattached dopamine molecules and then dried under a N_2 stream. The disks were then immersed in a solution of adhesion peptides (fibronectin sequences: KGGRGDSP and c(RGDfK); 1 mg mL^{-1} in 10 mM Tris buffer, pH 8.5, Chinese Peptide Company, China, ESI Fig. 1†) at room temperature for 24 h. Then, the disks were sterilized with 75% ethanol for 40 min and washed thrice with phosphate-buffered saline (PBS) before use. The substrates were designated ZrO_2 (pristine zirconia), ZrO_2-P (PDA-modified zirconia), and ZrO_2-P/L (linear peptides, KGGRGDSP-functionalized zirconia) and ZrO_2-P/C (cycle peptides, c(RGDfK)-functionalized zirconia). To confirm peptide conjugation, PDA-coated disks were immersed in fluorescein isothiocyanate (FITC)-labeled KGGRGDSP or c(RGDfK) solution at room temperature for 24 h and then in 75% ethanol solution for 40 min, followed by three washes with PBS. Fluorescence images were acquired using a confocal laser scanning microscope (CLSM; LSM710, Zeiss, Oberkochen, Germany) before and after sterilization/rinsing of the modified substrates.

2.3. Surface characterization

2.3.1. Surface topography and roughness. Surface topography was observed by atomic force microscopy (AFM; Dimension Icon, Bruker, Billerica, MA, USA) and scanning electron microscopy (SEM; S-4800, Hitachi, Tokyo, Japan). Peak-to-valley surface roughness (R_a) was determined by AFM. Three samples per group were observed in five random fields per sample.

2.3.2. Surface wettability. Surface wettability was evaluated by measuring the contact angle of a 1 μL droplet of double-distilled water using a contact angle meter (SL200, Kino Industry Co., Ltd, Boston, MA, USA). Measurements were taken at three different locations on each one of three samples per group.

2.3.3. Chemical composition. The chemical composition of the surfaces was analyzed by X-ray photoelectron spectroscopy (XPS; ESCALAB 250, Thermo Fisher Scientific, Waltham, MA, USA). Binding energies were referenced to the C 1s hydrocarbon peak at 284.6 eV.

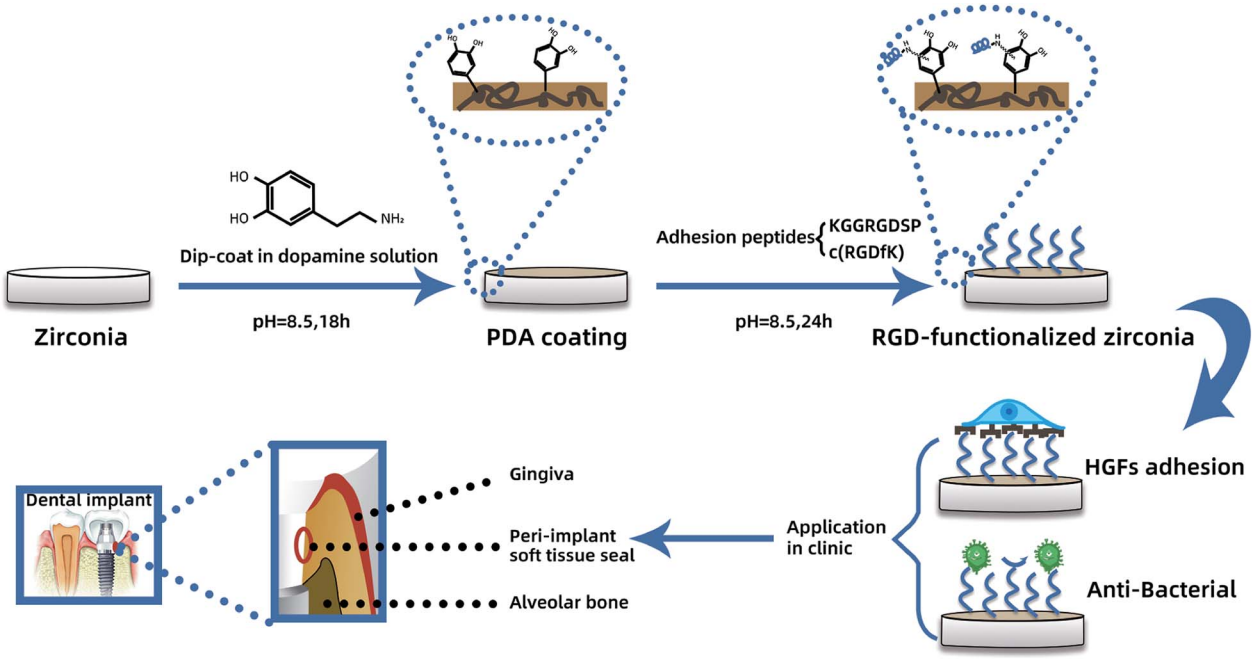

Scheme 1 PDA-mediated RGD functionalization process and its effect on HGFs and bacterial adhesion for enhanced peri-implant soft tissue seal.

2.4. Cellular responses

2.4.1. Cell culture. HGFs were derived from biopsies obtained from a periodontally healthy human subject during periodontal surgery, as previously described.[34] Cell collection was approved by the Ethics Committee of Peking University School and Hospital of Stomatology, and written informed consent was obtained from the patient. The HGFs were cultured in Dulbecco's modified Eagle's medium (Thermo Fisher Scientific, Gaithersburg, MD, USA) supplemented with 10% fetal bovine serum (Thermo Fisher Scientific, Gaithersburg, MD, USA) and 1% antibiotic-antimycotic solution (Thermo Fisher Scientific, Gaithersburg, MD, USA) at 37 °C under a humidified atmosphere of 5% CO_2 and 95% air. The culture medium was changed every other day. Confluent cells were subcultured by trypsinization. Cells from passages 3 to 7 were used in the experiments.

2.4.2. Cell adhesion and spreading. HGFs were seeded onto the surfaces of disks in a 24-well plate at a density of 1.0×10^5/well. After culturing for 3 h and 24 h, unattached cells were removed by rinsing with 1 mL PBS thrice. The attached cells were fixed with 4% paraformaldehyde at room temperature for 10 min. Subsequently, the cells were permeabilized in 0.1% Triton X-100 for 7 min, and then blocked with 1% bovine serum albumin (Sigma, St. Louis, MO, USA) for 15 min to prevent non-specific binding. After extensive rinsing with PBS (3 × 5 min each), the disks were stained with FITC-phalloidin (actin filaments, green color; 1 : 300, Sigma, St. Louis, MO, USA) for 1 h. Finally, nuclei were counterstained with a drop of Fluoroshield containing 4′,6-diamidino-2-phenylindole (blue color; Sigma, St. Louis, MO, USA). Coverslips were mounted on the surfaces, and the cells were observed by CLSM. Attached cells, projected area, and perimeter of HGFs were quantified using ImageJ (version 2, NIH, USA).

2.4.3. Cell proliferation. A Cell Counting Kit-8 (CCK-8; Dojindo, Kyushu, Japan) was used to quantify HGF proliferation. Cells were seeded on modified/unmodified zirconia disks at a density of 1.0×10^4/well. After incubation for 1, 3, or 5 days, the samples were washed thrice with PBS. CCK-8 solution diluted with cell culture medium (1 : 9, v/v) was added to each well, and the plate was incubated at 37 °C for 2.5 h. The supernatant was then transferred from the 24-well to a 96-well cell culture plate and the absorption at 450 nm was measured using a spectrophotometer (ELX808, BioTek, Winooski, VT, USA).

2.4.4. Gene expression analysis. Relative gene expression levels of integrin α5, integrin β1, focal adhesion kinase (FAK), vinculin (VCL), fibronectin (FN), and human collagen type I (Col-1) in HGFs seeded on zirconia disks of different groups were determined by quantitative reverse-transcription polymerase chain reaction (RT-qPCR). Total mRNA was extracted from 1 day cultures using TRIzol reagent (Invitrogen, Grand Island, NY, USA), and cDNA was generated using the RevertAid First Strand cDNA Synthesis Kit (Thermo Fisher Scientific, Waltham, MA, USA) according to the manufacturer's instructions. qPCRs were run using Power SYBR Green PCR Master Mix (Thermo Fisher Scientific, Waltham, MA, USA) and specific primers (Table 1) on a 7500 Real-time PCR System (Thermo Fisher Scientific, Waltham, MA, USA). *GADPH* was used as the reference gene. Relative expression levels were calculated using the $2^{-\Delta\Delta C_T}$ method and are presented as fold differences relative to the control group.

2.4.5. Protein determination. Col-1 secretion by HGFs after 3 and 7 days of incubation was quantified using an enzyme-linked immunosorbent assay kit (ELISA; R&D Systems, Minneapolis, MN, USA) according to the manufacturer's protocol. In brief, cell culture supernatants were collected and centrifuged at 3000 × *g* at 4 °C for 10 min to remove particles and polymer. In each well of a 96-well plate, 10 μL of sample, 40 μL of sample diluent, and 100 μL of HRP-conjugate reagent were added, followed by incubation at 37 °C for 1 h. After rinsing the wells with washing buffer five times, 50 μL of chromogen solutions A and B were added into each well, and the plate was incubated at 37 °C in the dark for 15 min. Finally, 50 μL of stop solution was added to each well to terminate the reaction. Absorbance at 450 nm was measured using a microplate reader and was used to estimate the protein concentration of the samples.

2.5. Bacterial responses

2.5.1. Saliva coating of zirconia disks. Saliva was collected from seven healthy donors as described previously,[34] and was centrifuged at 3000 rpm at 4 °C for 20 min to remove impurities. The clarified saliva was diluted with distilled water at a volume ratio of 1 : 3, passed through a 0.20 μm filter, and stored at −80 °C until use. Immediately before use, the frozen saliva was thawed in a water bath at 37 °C and centrifuged at 1430 × *g* for 5 min to obtain clear supernatant. Zirconia disks were immersed in the clear supernatant at 37 °C for 4 h to form a saliva film for bacterial adhesion.

2.5.2. Bacterial cultures. The antimicrobial activity of modified/unmodified samples was evaluated using Gram-positive *Streptococcus mutans* (strain UA159, provided by the Institute of Microbiology at the Chinese Academy of Sciences) and Gram-negative *Porphyromonas gingivalis* (strain W83, provided by the Central Laboratory of Peking University School of Stomatology). *S. mutans* and *P. gingivalis* were maintained on brain heart infusion agar plates (BHI, BD-Difco, Franklin, NJ, USA). *S. mutans* was maintained at 37 °C in a humidified atmosphere of 5% CO_2 and 95% air. *P. gingivalis* was maintained under standard anaerobic conditions (80% N_2, 10% H_2, 10% CO_2), at 37 °C. Monoclonal strains of the two species were separately transferred into 1 mL of liquid BHI medium and cultured to the exponential phase for use. Bacterial cells were centrifuged at 3000 × *g* for 15 min, and the cell pellet was washed twice with 0.15 M PBS buffer. The cells were resuspended at different final concentrations. Before seeding, the suspension was shaken for 30 s to obtain single cells or pairs. Cells were seeded on sterile samples in a 24-well plate for further experiments.

2.5.3. Bacterial adhesion. Bacteria (1×10^8 CFU mL^{-1}) were cocultured with saliva-coated zirconia disks for 3 h (*S. mutans*) or 48 h (*P. gingivalis*) for SEM and CLSM observation. After removing the culture medium, the cells were gently

Table 1 Primer pairs used in real-time PCR analysis

	Sequences (5′-3′)	
Gene	Forward	Reverse
Integrin α5	GGCAGCTATGGCGTCCCACTGTG	GGCATCAGAGGTGGCTGGAGG
Integrin β1	CAAAGGAACAGCAGAGAAGC	ATTGAGTAAGACAGGTCCATAA
Fibronectin	CGGAGAGACAGGAGGAAATAGCC	TTGCTGCTTGCGGGGCTGTC
Focal adhesion kinase	CTCCTACTGCCAACCTGGAC	GCCGACTTCCTTCACCATAG
Vinculin	CGAATCCCAACCATAAGCAC	CGCACAGTCTCCTTCACAGA
Collagen type I	AGAGCATGACCGATGGATTC	TTCTTGAGGTTGCCAGTC
GAPDH	TGCACCACCAACTGCTTAGC	GGCATGGACTGTGGTCATGAG

washed with sterile PBS to remove non-attached cells. Adherent bacteria on the disks were fixed with 2.5% glutaraldehyde at room temperature for 60 min. After three washes with PBS, the disks were dehydrated in a graded series of ethanol (25%, 50%, 70%, 90%, 95%, and 100%) for 10 min. Finally, the disks were dried, sputter-coated with gold, and imaged by SEM.

The LIVE/DEAD BacLight Bacterial Viability Kit (Invitrogen, Carlsbad, CA, USA) was used to examine live (green-fluorescent) and dead (red-fluorescent) bacteria. The staining components A (SYTO 9) and B (propidium iodide) were mixed and diluted in PBS at a volume ratio of 1.5 : 1000 according to the manufacturer's instructions. Three hundred microliters of mixed staining dilution was added to each sample, followed by incubation at 37 °C in the dark for 15 min. The stained bacteria were observed by CLSM. Digital images were acquired for five random fields on each surface. The percentage of area covered by bacteria in each image was quantified using Image J software.

2.6. Statistical analysis

All experiments were performed three times independently, in triplicate. All data are expressed as the mean ± standard deviation (SD). Statistical analysis was performed using one-way analysis of variance (ANOVA) followed by Tukey tests. $p < 0.05$ was considered statistically significant.

3. Results and discussion

3.1. Functionalization characterization

The topographies of pristine and decorated zirconia were observed by SEM and AFM (Fig. 1). Self-polymerized PDA particulates were observed on the ZrO_2-P surface. Immobilization of KGGRGDSP and c(RGDfK) peptides increased the PDA particulate size, suggesting that RGD peptides were successfully grafted onto the zirconia substrate surface. Surface roughness was determined by AFM (Table 2). After PDA coating, the R_a value increased slightly, albeit not significantly, from 0.207 ± 0.009 μm to 0.217 ± 0.005 μm. Chemical coupling of RGD peptides on the ZrO_2-P surface did not affect the R_a values (0.222 ± 0.008 μm for ZrO_2-P/L and 0.214 ± 0.008 μm for ZrO_2-P/C). Surface topography is a key factor affecting the biological responses of host cells and bacteria.[38] Abutment surfaces with micro-roughness (3–30 μm) have been suggested to inhibit epithelial down growth,[39] whereas bacterial colonization increased with a roughness >0.2 μm.[40] Taking these factors into account, Gehrke *et al.* proposed an abutment-surface-roughness classification method for clinical practice, and determined the optimal surface roughness for the trans-mucosal portion of implant abutments that strikes a balance between soft tissue sealing and bacterial adhesion to be 0.15–0.25 μm.[41] Therefore, the zirconia disks used in this study were polished to 0.2 μm to mimic the transgingival surface of commercially available zirconia abutments. The R_a values did not significantly differ between unmodified and modified zirconia, indicating that changes in cellular response and bacterial colonization on different substrates might have little to do with surface roughness.

Surface wettability of pristine and decorated zirconia substrates was determined by water contact angle measurements (Table 2). After PDA deposition, the contact angle significantly decreased from 72.8 ± 2.3° to 61.9 ± 2.6° ($p < 0.05$). Immobilization of RGD peptides onto the ZrO_2-P surface further decreased the contact angle (46.5 ± 1.4° on ZrO_2-P/L and 45.2 ± 2.2° on ZrO_2-P/C), likely because of the hydrophilic groups (–OH, –COOH, and $–NH_2$) of the grafted peptides. These gradual changes in the static contact angle indicated successful PDA coating and functionalization with RGD peptides. Surface wettability is another pivotal factor influencing peri-implant soft tissue integration. Kloss *et al.* reported that hydrophilic surfaces promoted connective tissue attachment and cell–surface contacts, and suppressed inflammatory responses.[42] In the present study, surface wettability increased after the grafting of RGD peptides. Thus, immobilization of KGGRGDSP and c(RGDfK) on zirconia abutments may promote soft tissue healing.

Stable immobilization of RGD peptides onto the substrate is crucial for promoting strong cell adhesion, as focal adhesion formation occurs only when the ligands can withstand cell contractile forces.[43] These forces can redistribute weakly adsorbed ligands on the substrate, leading to weak fibrillar adhesions.[44] Thus, for stable linkage, the RGD peptides should ideally be covalently attached to the substrate. We investigated RGD peptide immobilization by using FITC-labeled KGGRGDSP and c(RGDfK) peptides that were chemically coupled to ZrO_2-P surfaces. Fig. 2 shows fluorescence images of CLSM of the substrate surfaces. Before RGD coating, there was almost no

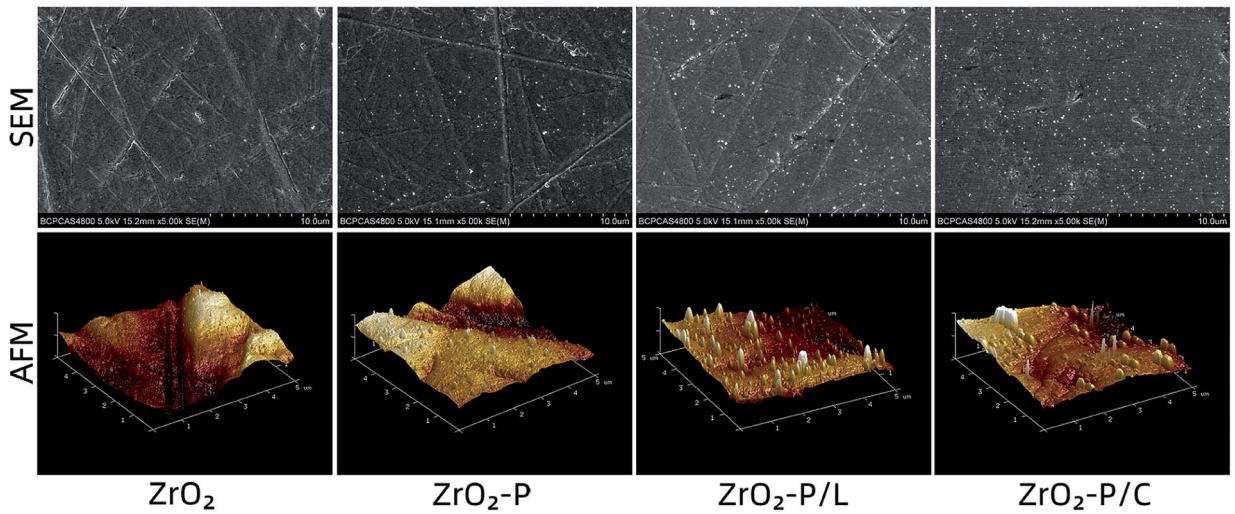

Fig. 1 Surface topography of zirconia substrates: AFM and SEM images of the pristine zirconia, PDA-coated zirconia, and RGD-functionalized zirconia.

noticeable fluorescent signal on ZrO_2 and ZrO_2-P surfaces. In contrast, after grafting RGD on PDA film, punctate green fluorescence was observed on the ZrO_2-P/L and ZrO_2-P/C surfaces. After immersing the disks of ZrO_2-P/L and ZrO_2-P/C in 75% alcohol solution for 40 min and washing them thrice with PBS, the fluorescence was slightly reduced, but still visible. RGD peptides physically adsorbed on the surface were washed away after alcohol immersion and multiple washing steps; the remaining peptides were covalently coupled onto the PDA coating.

The atomic chemical composition of the functionalized zirconia surfaces was analyzed by XPS. The wide scan spectra of the various surfaces are shown in Fig. 3A. ZrO_2 substrate displayed strong Zr 3d, O 1s, and C 1s peaks. The presence of PDA on the zirconia surface could be deduced from the appearance of the N 1s peak and the decrease of the Zr 3d peak.[34] Following RGD immobilization, the N 1s peak strongly increased, indicating successful anchoring of the cell adhesion peptides. These results were confirmed by elemental percentage changes summarized in Fig. 3B. The nitrogen content was strongly increased after RGD modification (from 3.42% on ZrO_2 and 6.56% on ZrO_2-P to 13.02% on ZrO_2-P/L and 13.85% on ZrO_2-P/C) because of the amine groups and peptide bonds in the peptides. To obtain the detailed chemical composition of each sample, C 1s peak fitting was further analyzed (Fig. 3C). The high-resolution C 1s spectrum of ZrO_2 was deconvoluted into three curves with binding energy at 284.8 eV (C–C/C–H), 286.5 eV (C–O), and 288.8 eV (C═O). After PDA coating, the C–O and C═O peaks were increased, whereas the C–C/C–H peak was

Table 2 Quantitative measurement of water contact angle and surface roughness

	Roughness (μm)	Water contact angle (°)
ZrO_2	0.207 ± 0.009	72.8 ± 2.3
ZrO_2-P	0.217 ± 0.005	61.9 ± 2.6
ZrO_2-P/L	0.222 ± 0.008	46.5 ± 1.4
ZrO_2-P/C	0.214 ± 0.008	45.2 ± 2.2

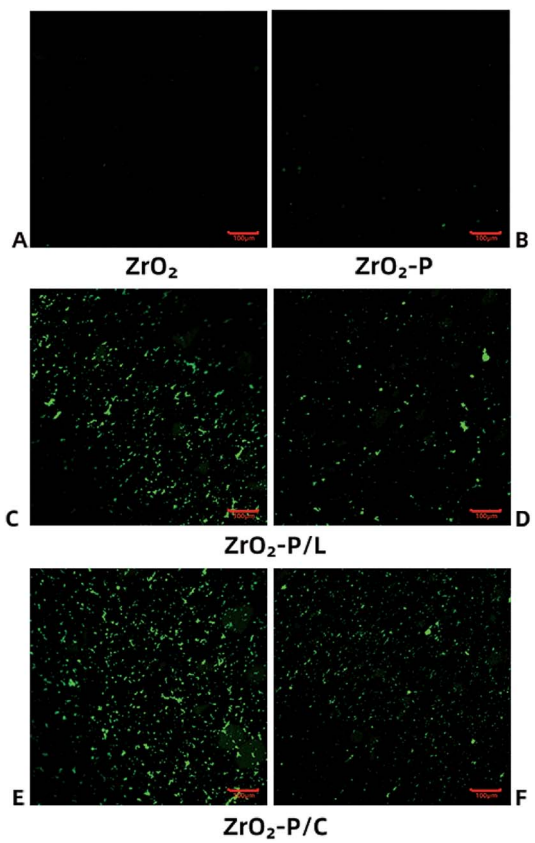

Fig. 2 No noticeable fluorescent signal was observed on ZrO_2 (A) and ZrO_2-P (B) surfaces. Punctate green fluorescence was observed on the ZrO_2-P/L (C) and ZrO_2-P/C (E) surfaces. Reduced green fluorescence were observed on ZrO_2-P/L (D) and ZrO_2-P/C (F) surfaces after rinsing.

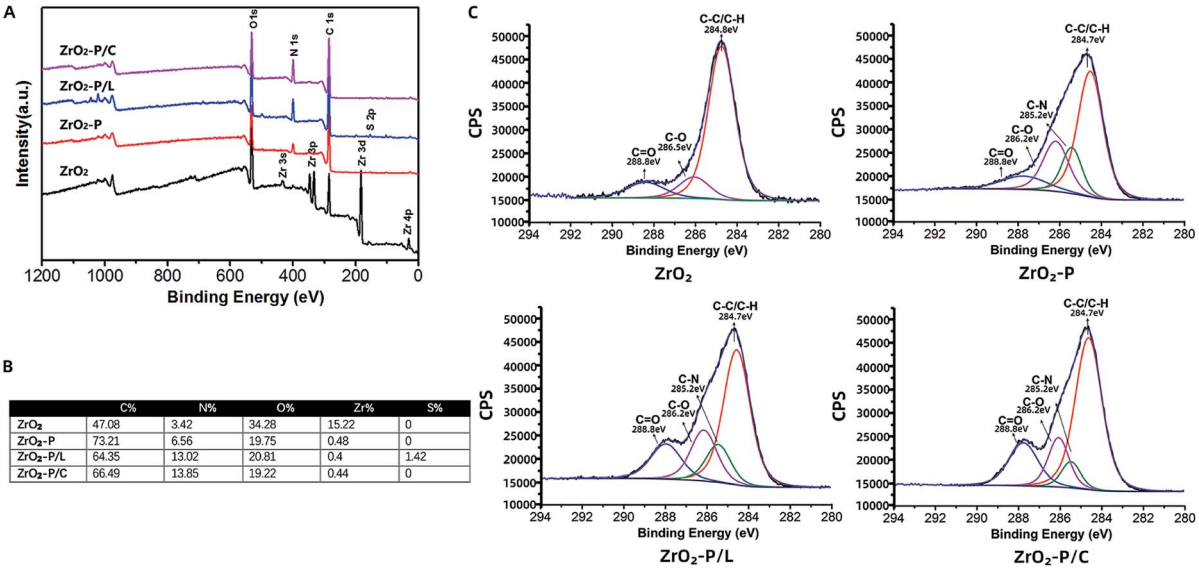

	C%	N%	O%	Zr%	S%
ZrO_2	47.08	3.42	34.28	15.22	0
ZrO_2-P	73.21	6.56	19.75	0.48	0
ZrO_2-P/L	64.35	13.02	20.81	0.4	1.42
ZrO_2-P/C	66.49	13.85	19.22	0.44	0

Fig. 3 (A) XPS wide-scan spectra of different groups; (B) quantification in (%) of atomic compositions on the unmodified and modified zirconia surfaces; (C) typical high-resolution XPS C 1s spectra for different substrates. The ordinate CPS (counts per second) represents the relative photoelectron intensity.

dramatically decreased, which is attribute to the catechol/quinone groups of PDA. Compared with that of ZrO_2-P, the C═O peak was significantly increased after RGD peptide grafting due to abundant amide bonds (–NH–C═O). Together, these results suggested that RGD peptides can be covalently immobilized onto zirconia surfaces *via* PDA coating.

3.2. HGF responses

3.2.1. HGF adhesion, spreading, and proliferation. As one of the major cells of peri-implant soft tissue, HGFs synthesize and maintain the ECM, which plays a primary role in tissue repair and regeneration during wound healing.[45] Therefore, enhancing the biological response of HGFs by modifying the zirconia abutment surface might improve peri-implant soft tissue closure. When implant is placed into a host and comes into contact with HGFs, the initial step is cell attachment, which is crucial for subsequent cellular behaviors, such as spreading, proliferation, and differentiation.[44] We employed CLSM to observe the adhesion and morphology of HGFs on pristine and modified zirconia surfaces (Fig. 4). At 3 h after cell seeding, HGFs on ZrO_2 were round-shaped, with few cellular processes—

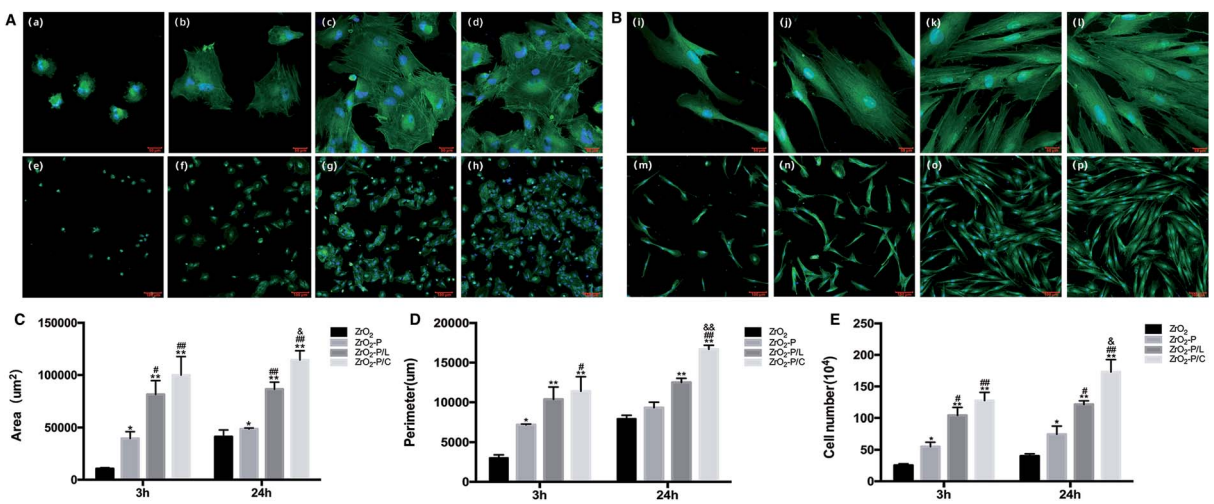

Fig. 4 Confocal laser scanning microscopy images of HGFs on pristine zirconia (a, e, i, m), ZrO_2-P (b, f, j, n), ZrO_2-P/L (c, g, k, o), and ZrO_2-P/C (d, h, l, p) surfaces after 3 h (A) and 24 h (B) of culture. High magnification (a, b, c, d, i, j, k, l): scale bar = 20 μm; low magnification (e, f, g, h, m, n, o, p): scale bar = 100 μm. Quantitative results for spreading areas (C), perimeters (D), and numbers (E) of HGFs cultured for 3 h and 24 h on different substrates. Data are shown as mean ± SD ($n = 15$). * represents $p < 0.05$ and ** represents $p < 0.01$, compared with pristine zirconia. $^{\#}$ represents $p < 0.05$ and $^{\#\#}$ represents $p < 0.01$, compared with ZrO_2-P. $^{\&}$ represents $p < 0.05$ and $^{\&\&}$ represents $p < 0.01$, compared with ZrO_2-P/L.

a typical non-spreading morphology. Cells cultured on ZrO_2-P surfaces for 3 h had spread over a larger area. On ZrO_2-P/L and ZrO_2-P/C surfaces, the cells had spread more extensively, and filopodium-like processes appeared. Subsequently, cell membrane protrusions formed further, resulting in rapid cell spreading and formation of bridge connections between adjacent cells on the modified zirconia surfaces after 24 h of incubation, particularly in the ZrO_2-P/L and ZrO_2-P/C groups. In comparison, cells cultured on ZrO_2 surfaces had a spindle-like and narrow shape, with fewer protrusions, and there were fewer cells. The differences observed in cell attachment and morphology were quantified by counting adhered cells and measuring their area and perimeter (Fig. 4C–E). HGF number, projected area, and perimeter were all increased after PDA coating, which was consistent with findings in our previous study.[34] RGD functionalization further increased the adhesion and spreading of adherent cells at both 3 h and 24 h. Cell number, projected area, and perimeter were the highest on ZrO_2-P/C, indicating a high degree of adhesion and spreading. These results indicated that PDA-mediated functionalization of zirconia substrates with RGD peptides, especially cyclic peptides, promotes HGF attachment and spreading.

The proliferation of HGFs cultured on the different substrates was detected by CCK-8 assay on days 1, 3, and 5 (Fig. 5). The proliferation of adhered HGFs increased with increasing culture time in all groups. There were no statistically significant differences among the four groups on day 1. On days 3 and 5, proliferation was the highest on RGD-decorated surfaces, followed by ZrO_2-P, and then ZrO_2. HGF proliferation was higher on ZrO_2-P/C than on ZrO_2-P/L, especially after 5 days ($p < 0.05$). These results indicated that RGD peptides effectively stimulate HGF proliferation, with cyclic performing slightly better than linear peptides.

3.2.2. Gene expression and protein synthesis in HGFs. Integrin-mediated cell adhesion comprises several cascade events: cell attachment, cell spreading, organization of the actin cytoskeleton, and formation of focal adhesions.[46] Integrins are a family of transmembrane glycoprotein receptors that regulate cell adhesion by attaching intracellular cytoskeletal elements to extracellular molecules. RGD sequence, as the central cell binding domain of FN, can bind cell membrane integrins and thus mediate cell adhesion.[47] Integrin α5β1 is a key receptor of RGD and plays a predominant role in fibroblast adhesion.[48] Thus, RGD peptide modification of zirconia surfaces might enhance the affinity of HGFs towards the substrate *via* α5β1–RGD interactions. Moreover, the binding of α5β1 and FN mediates FN fibril formation and controls ECM assembly, which is critical for cellular function *in vivo*.[49] Indeed, FN, which is abundantly expressed by fibroblasts, can modulate several physiological and pathological processes, including tissue repair and wound healing.[50] According to RT-qPCR results (Fig. 6), gene expression of integrin α5 in HGFs was increased on ZrO_2-P compared to ZrO_2 ($p < 0.05$), consistent with previous findings,[34] and even more so on ZrO_2-P/L and ZrO_2-P/C ($p < 0.01$), while there was no significant difference between the two RGD peptides ($p > 0.05$). Integrin β1 gene expression was increased after PDA and RGD modifications, and significantly so on ZrO_2-P/C ($p < 0.05$). FN gene expression was significantly higher on ZrO_2-P and ZrO_2-P/C than on ZrO_2 ($p < 0.01$). These results implied that PDA-mediated RGD immobilization might promote early adhesion of HGFs by stimulating integrin expression and ECM secretion. The binding of integrins to RGD-containing ECM proteins leads to the assembly of focal adhesions (FAs), which play a crucial role in cellular adhesion and sensing of the external environment. FAs are closed junctions between the cell and a substrate, where integrins link the ECM to the actin cytoskeleton. Among the three main ways of contact between fibroblasts and substrate materials, *i.e.*, FAs, close contacts, and ECM contacts, FAs are considered to be the tightest.[51] FAs not only transmit force at adhesion sites to maintain strong attachments to the ECM, but also act as signaling centers from which numerous intracellular pathways emanate to regulate cell behaviors.[52] During FA assembly, integrins cluster into supramolecular complexes with signaling molecules such as focal adhesion kinase (FAK), as well as structural proteins such as vinculin. FAK is a vital non-receptor tyrosine kinase that regulates cell adhesion signaling and mechanosensing.[53] Vinculin is a key regulator of adhesion

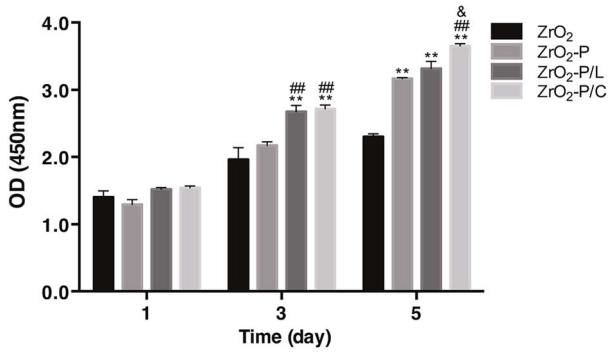

Fig. 5 The proliferation of HGFs cultured on different substrates for 1, 3, and 5 days was evaluated by CCK-8 assay. * represents $p < 0.05$ and ** represents $p < 0.01$, compared with pristine zirconia. ## represents $p < 0.01$, compared with ZrO_2-P. & represents $p < 0.05$, compared with ZrO_2-P/L.

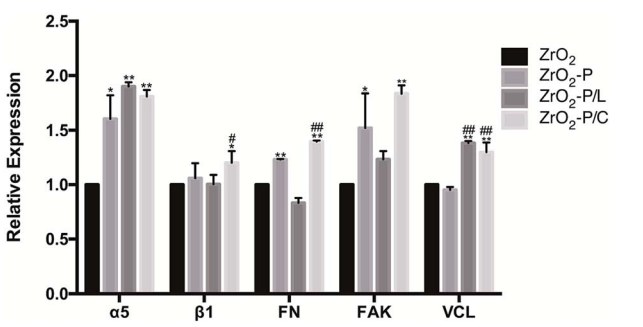

Fig. 6 Analyses on the expressions of genes involved in HGFs adhesion after 24 h of culture in real-time PCR. Data represent fold changes of target genes relative to the GAPDH expression and the HGFs grew on pristine zirconia (100%). * represents $p < 0.05$ and ** represents $p < 0.01$, compared with pristine zirconia. # represents $p < 0.05$ and ## represents $p < 0.01$, compared with ZrO_2-P.

strength and cell migration.[54] FAK gene expression in HGFs was increased in all three experimental groups when compared with the control group, particularly on ZrO_2-P/C ($p < 0.01$) and ZrO_2-P ($p < 0.05$). Vinculin gene expression was significantly higher on ZrO_2-P/C and ZrO_2-P-L than on ZrO_2 ($p < 0.01$), indicating that FA assembly might be promoted. These findings implied that the immobilized RGD peptides enhanced the interaction between HGFs and zirconia surfaces, which might provide a foundation for strong adhesion of HGFs and subsequently tight sealing of soft tissue around zirconia abutments in clinic.

HGFs participate in the formation of connective tissue around an implant during wound healing by producing ECM factors such as collagen type I (Col-1).[55] We quantified Col-1 expression at both the gene and protein levels to investigate the functional development of HGFs on the different modified surfaces (Fig. 7). After 3 days of incubation, Col-1 gene expression was similar among all substrates, whereas protein expression was slightly higher on ZrO_2-P/L and especially, ZrO_2-P/C, than in the control group ($p < 0.05$). The difference between the two RGD peptides was not significant ($p > 0.05$). After 7 days of culture, higher Col-1 gene and protein expression were observed in all functionalized groups, and particularly, significant differences were observed for ZrO_2-P/L ($p < 0.01$ at the gene level and $p < 0.05$ at the protein level). In addition, HGFs cultured on ZrO_2-P/L displayed higher Col-1 gene expression than those cultured on ZrO_2-P/C for 7 days. These results suggested that KGGRGDSP and c(RGDfK) promote Col-1 secretion. Moreover, cyclic and liner RGD peptides promote cell differentiation in a similar manner, with only subtle evidence of superiority of the linear RGD modification.

RGD-containing peptides are commonly utilized to direct cell adhesion behaviors on biomaterials.[56] Depending on the spatial structure, they are divided into linear and cyclic peptides. Cyclic peptides mimic the active conformation of the bound form and have a 20–100 fold stronger affinity for integrins than linear RGD peptides, especially for αVβ3, αIIβ3, and αvβ5.[44] Moreover, the ring structure increases the rigidity of the peptide and protects it from degradation.[57] In comparison, linear peptides, such as GRGDSP, have comparable affinity to α5β1, αVβ3, and αIIβ3 at an intermediate level.[46] Different conformations of immobilized RGD promote differential cell type-dependent responses to material surfaces. As for bone-related cells, cyclic RGD peptides have been extensively employed, and they are more effective in improving osteoblast behavior and stimulating peri-implant bone formation than linear RGD peptides.[21] However, as for soft tissue healing, conflicting results on the effects of cyclic and linear RGD peptides on fibroblasts have been reported. Kato *et al.* found that 3T3 Swiss fibroblasts adhered approximately two times faster to cyclic RGDfK than to linear RGDS, and more, but smaller focal contacts were formed when the cyclic peptide was used.[58] Wohlrab *et al.* reported that the binding activity of a linear RGD (in a genetically engineered hybrid silk protein) to BALB/3T3 fibroblasts was indistinguishable from that of a cyclic RGD (chemically coupled to the silk protein).[59] However, Massia *et al.* found that fibroblast attachment was higher on an α5β1 integrin-selective GRGDSP peptide-functionalized surface than on a surface modified with cyclic GpenGRGDSPCA.[60] In the present study, we compared the effects of KGGRGDSP and c(RGDfK) on HGF biological behaviors. CLSM and CCK-8 assays indicated that c(RGDfK) promoted slightly better cell adhesion, spreading, and proliferation than did KGGRGDSP. However, gene and protein expression analyses indicated that the linear and cyclic peptides induced Col-1 secretion to comparable levels. These findings could be interpreted as follows: the linear GRGDSP-containing peptide and the c(RGDfK) peptide have similar affinity for α5β1 integrin, which is critical for fibroblasts to bind and respond to the ECM, whereas the cyclic peptide has higher affinity for other integrins, and the cell behaviors reflect the summation of different binding affinities. Further, cell adhesion depends also on the density of immobilized peptides.[61] Small changes in peptide density can have dramatic effects in terms of their functions. The two RGD peptides in this study were grafted onto the zirconia surfaces at the same concentration, and their density was neither the same nor constant. As shown in Fig. 2, more punctate green fluorescence was observed on ZrO_2-P/C than on ZrO_2-P/L surfaces, indicating the higher density of c(RGDfK). This difference in density may partly explain the differential effects of ZrO_2-P/C and ZrO_2-P/L on cell activity. In addition, the linear RGD peptide has probably no conformation like the cyclic RGD peptide. The PDA-mediated RGD immobilization was carried out in aqueous solutions, the conformation of the peptides was hardly destroyed, thus retaining their receptor-binding capability and biological activity to the most extent.

3.3. Bacterial responses

CLSM and SEM images of the colonization of *S. mutans* and *P. gingivalis* on the different substrates are shown in Fig. 8A and B.

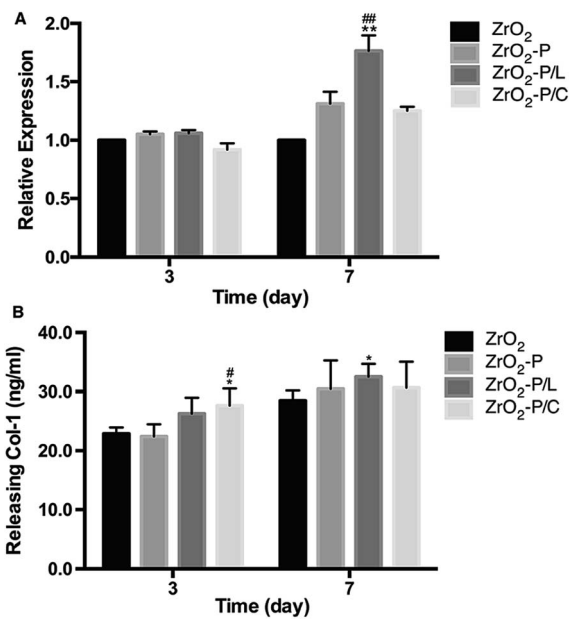

Fig. 7 The expression of Col-1 at gene (A) and protein (B) levels after 3 and 7 days of culture. * represents $p < 0.05$ and ** represents $p < 0.01$, compared with pristine zirconia. # represents $p < 0.05$ and ## represents $p < 0.01$, compared with ZrO_2-P.

The adhesion density of *S. mutans* as well as *P. gingivalis* (sum of live and dead cells in CLSM) was decreased on ZrO_2-P, ZrO_2-P/L, and ZrO_2-P/C as compared with ZrO_2. ZrO_2-P, ZrO_2-P/L, and ZrO_2-P/C reduced bacterial adhesion to the same extent. CLSM revealed more dead cells of *S. mutans* on ZrO_2-P, ZrO_2-P/L and ZrO_2-P/C than on ZrO_2. The percentage of bacterial adhesion area to the tested surfaces is shown in Fig. 8C and D. Consistent with these qualitative microscopic impressions, the area coverages of *S. mutans* on all the modified substrates were significantly lower than on the pristine zirconia surfaces after 3 h of culture ($p < 0.01$); the differences between experiment groups were not significant. Similar results were found for *P. gingivalis* after incubation for 48 h.

As the oral environment is rich in bacteria, including potential pathogens, the antimicrobial property of dental implants is critical. Early failure of dental implants is often caused by the adhesion of *S. mutans* and other initial colonizers, which prevent the formation of soft tissue seal.[62] *P. gingivalis* is one of the major pathogens causing peri-implantitis, and plays an important role in regulating biofilm structure and toxicity and subsequent tissue inflammation.[63] Bacterial infection starts at the implant collars and then spreads along the bone-implant interface, resulting in failure of osseointegration.[64] Thus, inhibiting bacterial adhesion on the neck portion of the implant at the early stage would be of great significance.

Bacterium-surface adhesion is determined by various surface physicochemical properties, such as roughness, wettability, surface charge, and chemical composition. Surface roughness plays a vital role in bacterial adhesion. As mentioned above, all samples in this study had a surface roughness of approximately 0.2 μm; therefore, roughness does not explain the differences in bacterial adhesion. Further, hydrophilic materials are more resistant to bacterial adhesion than hydrophobic materials.[65] In this study, the water contact angle was decreased by 11° after PDA coating, and by 16° after RGD functionalization. The enhanced hydrophilicity may account, at least in part, for the decrease in bacterial colonization on modified samples. Surface charge is another crucial physical factor influencing the adherence of microorganisms, *e.g.*, most bacteria are negatively charged and preferentially adhere to positively charged surfaces. The antimicrobial activity of RGD peptides has been rarely explored. ECM proteins such as collagen and FN contain specific bacterial binding sites; however, few bacteria have been identified to bind directly to sequences containing a single RGD motif.[66] In a study

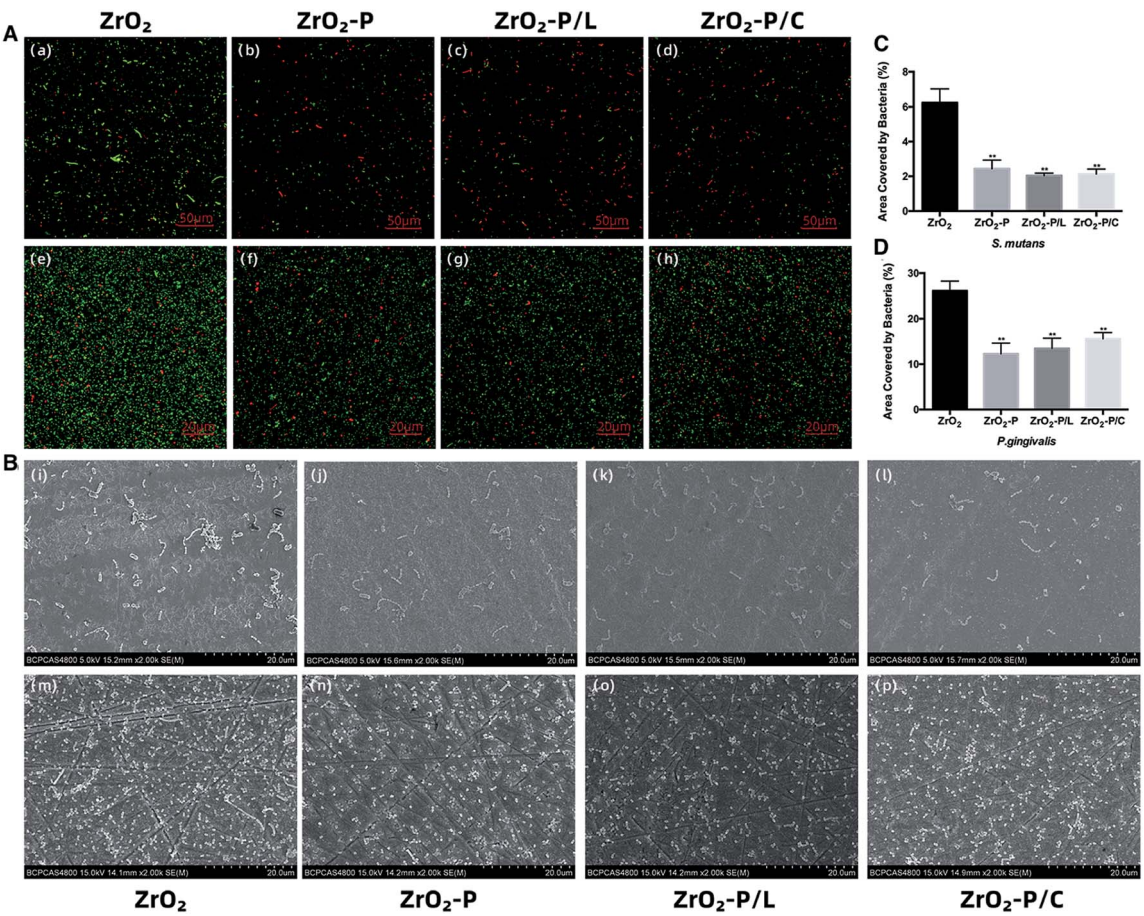

Fig. 8 CLSM (A) images of *S. mutans* after 3 h of culture (A(a–d) scale bar = 50 μm) and *P. gingivalis* after 48 h of culture (A(e–h) scale bar = 50 μm) on different surfaces. SEM (B) images of *S. mutans* after 3 h of culture (B(i–l)) and *P. gingivalis* after 48 h of culture (B(m–p)) on different surfaces. (C) and (D) Comparison of the area covered by bacteria among unmodified and modified substrates by CLSM images ($n = 15$). ** represents $p < 0.01$, compared with pristine zirconia.

by Chua *et al.*, RGD modification did not affect the antibacterial efficacy of hyaluronic acid/chitosan polyelectrolyte multilayer coating.[67] Similar findings have been reported in related studies on various bacterial strains.[68–70] Our findings are consistent with those in previous reports. The extent of bacterial adhesion on PDA-modified surfaces with or without immobilized RGD was significantly lower than that on pristine zirconia, and all modifications were similarly effective in reducing bacterial colonization; thus, the antibacterial effect was presumably largely contributed by PDA. However, results on the antimicrobial activity of PDA coating are controversial.[32] According to our previous work, PDA coating exerts a bacteriostatic effect on Gram-positive bacteria such as *Streptococcus gordonii* and *S. mutans*, probably because the negatively charged (pH > 4) and relatively hydrophilic PDA coating reduces the adhesion of negatively charged salivary proteins and subsequently, bacterial adhesion.[34] Also, Su *et al.* found that a roughened PDA, prepared by a facile shaking method, exhibited remarkable antibacterial activities against the Gram-positive *Staphylococcus aureus*, and the Gram-negative *Escherichia coli* and *Pseudomonas aeruginosa*.[71] Their findings suggested that modulation of the physical properties of PDA coating *via* the preparation conditions might significantly influence its antibacterial activity. The present study demonstrated that the presence of RGD did not influence the antimicrobial properties of PDA film. These findings can be explained as follows. The hydrophilicity was increased after immobilizing RGD peptides onto ZrO_2-P, which would have positively contributed to bacterial adhesion inhibition. However, this effect was likely cancelled out by the fact that RGD has a nearly zero net charge at neutral pH, and therefore, RGD conjugation might have affected the surface charge of the PDA film and thus, decreased its antibacterial activity.

Collectively, our findings indicate that PDA-mediated RGD functionalization greatly improved the early responses of HGFs, such as adhesion and spreading, while reducing the colonization of *S. mutants* and *P. gingivalis*. These results implied that soft tissue-related cells might have a competitive advantage over bacteria in occupying the zirconia abutment surface early after implantation and thus facilitate early soft tissue healing. Furthermore, enhanced HGF proliferation and differentiation on RGD-functionalized zirconia may promote the formation of an extensive and tight connective tissue seal on the transgingival area of the implant. Apart from the efficacy of the coating, long-term stability has to be considered. The PDA and RGD coatings might be degraded *in vivo* at some point in time by enzymatic activities or under oral physiological forces. However, as the coating is cell-adhesive and bacteria-repellent, HGFs have a considerably greater possibility to win the race-for-the-surface against oral bacteria. Thus, even with a limited lifetime, the coatings are expected to be useful in protecting the implant against bacterial infection in the clinically critical early stage. Nevertheless, further investigations are still needed to assess the longevity of the coatings.

4. Conclusions

In the present study, we described a facile and effective surface modification approach for zirconia abutment material, enabling covalently binding of RGD-containing peptides *via* PDA intermediate layer to significantly improve the biological activity of HGFs. In the comparison between liner and cyclic RGD, cyclic peptides promoted cell attachment, spreading, and proliferation slightly better than linear RGD peptide, whereas both peptides had comparable effects on cell differentiation. Moreover, RGD functionalization did not alter the antibacterial efficacy of PDA coating. Therefore, the zirconia-PDA-RGD surface exhibits selective bio-interactivity, *i.e.*, it is adhesive to soft tissue-forming cells, but repellent to bacteria, a property that holds promise for enhancing peri-implant soft tissue integration. Nevertheless, further studies *in vitro* and *in vivo* are necessary to establish the optimal application conditions of PDA-mediated RGD functionalization, and to assess its soft tissue healing-promoting effects *in vivo*.

Ethical statement

HGFs were grown from biopsies obtained from a periodontally healthy human subject during periodontal surgery. The process is with the advance approval of informed consent. Meanwhile, the study was approved by the Institutional Review Board of Peking University School of Stomatology (Beijing, China PKUSSIRB-201943032).

Conflicts of interest

We have no conflicts of interest for the study.

Acknowledgements

The study was supported by the National Natural Science Foundation of China (No. 81701001) and (No. 81701003).

References

1 T. Wang, L. Wang, Q. Lu and Z. Fan, *J. Prosthet. Dent*, 2019, **121**, 156–165.
2 F. Al Rezk, G. Trimpou, H. C. Lauer, P. Weigl and N. Krockow, *Gen. Dent.*, 2018, **66**, 18–25.
3 A. Sculean, R. Gruber and D. D. Bosshardt, *J. Clin. Periodontol.*, 2014, **41**(suppl. 15), S6–S22.
4 A. G. Gristina, *Science*, 1987, **237**, 1588–1595.
5 B. Zhao, H. C. van der Mei, G. Subbiahdoss, J. de Vries, M. Rustema-Abbing, R. Kuijer, H. J. Busscher and Y. Ren, *Dent. Mater.*, 2014, **30**, 716–727.
6 M. Rakic, P. Galindo-Moreno, A. Monje, S. Radovanovic, H.-L. Wang, D. Cochran, A. Sculean and L. Canullo, *Clin. Oral Invest.*, 2017, **22**, 1805–1816.
7 M. A. Pacha-Olivenza, R. Tejero, M. C. Fernandez-Calderon, E. Anitua, M. Troya and M. L. Gonzalez-Martin, *BioMed Res. Int.*, 2019, **2019**, 8456342.
8 B. Li, V. Agarwal, D. Ho, J.-P. Vede and K. S. Iyer, *New J. Chem.*, 2018, **42**, 7237–7240.
9 S. Roehling, K. A. Schlegel, H. Woelfler and M. Gahlert, *Clin. Oral Implants Res.*, 2019, **30**, 365–395.

10 L. Treccani, T. Yvonne Klein, F. Meder, K. Pardun and K. Rezwan, *Acta Biomater.*, 2013, **9**, 7115–7150.
11 M. Gahlert, T. Gudehus, S. Eichhorn, E. Steinhauser, H. Kniha and W. Erhardt, *Clin. Oral Implants Res.*, 2007, **18**, 662–668.
12 Q. Flamant, F. García Marro, J. J. Roa Rovira and M. Anglada, *J. Eur. Ceram. Soc.*, 2016, **36**, 121–134.
13 Y. Yang, J. Zhou, X. Liu, M. Zheng, J. Yang and J. Tan, *J. Biomed. Mater. Res. B Appl. Biomater.*, 2015, **103**, 116–124.
14 M. Zheng, Y. Yang, X. Q. Liu, M. Y. Liu, X. F. Zhang, X. Wang, H. P. Li and J. G. Tan, *PLoS One*, 2015, **10**, e0140278.
15 Y. Kimie, K. Kae, T. Yusuke, Y. Yuichiro and K. Hirofumi, *J. Hard Tissue Biol.*, 2014, **23**, 93–100.
16 Y. Cho, J. Hong, H. Ryoo, D. Kim, J. Park and J. Han, *J. Dent. Res.*, 2015, **94**, 491–499.
17 K. Pardun, L. Treccani, E. Volkmann, P. Streckbein, C. Heiss, G. Li Destri, G. Marletta and K. Rezwan, *Mater. Sci. Eng., C*, 2015, **48**, 337–346.
18 U. T. Kalyoncuoglu, B. Yilmaz, S. G. Koc, Z. Evis, P. U. Arpaci and G. Kansu, *Clin. Implant Dent. Relat. Res.*, 2018, **20**, 1022–1029.
19 C. M. Hsu, Y. S. Sun and H. H. Huang, *J. Dent. Res.*, 2019, **98**, 556–563.
20 F. Teng, Y. Zheng, G. Wu, B. Beekmans, D. Wismeijer, X. Lin and Y. Liu, *Int. J. Periodontics Restor. Dent.*, 2019, **39**, 371–379.
21 B. G. Zhang, D. E. Myers, G. G. Wallace, M. Brandt and P. F. Choong, *Int. J. Mol. Sci.*, 2014, **15**, 11878–11921.
22 N. Huettner, T. R. Dargaville and A. Forget, *Trends Biotechnol.*, 2018, **36**, 372–383.
23 J. W. Park, K. Kurashima, Y. Tustusmi, C. H. An, J. Y. Suh, H. Doi, N. Nomura, K. Noda and T. Hanawa, *Acta Biomater.*, 2011, **7**, 3222–3229.
24 H. S. Seo, Y. M. Ko, J. W. Shim, Y. K. Lim, J.-K. Kook, D.-L. Cho and B. H. Kim, *Appl. Surf. Sci.*, 2010, **257**, 596–602.
25 G. L. Yang, F. M. He, X. F. Yang, X. X. Wang and S. F. Zhao, *Int. J. Periodontics Restor. Dent.*, 2009, **90**, 175–185.
26 J. Michael, L. Schonzart, I. Israel, R. Beutner, D. Scharnweber, H. Worch, U. Hempel and B. Schwenzer, *Bioconjugate Chem.*, 2009, **20**, 710–718.
27 Y. Dong, P. Li, C. B. Chen, Z. H. Wang, P. Ma and G. Q. Chen, *Biomaterials*, 2010, **31**, 8921–8930.
28 W. C. Chen and C. L. Ko, *Mater. Sci. Eng., C*, 2013, **33**, 2713–2722.
29 M. Jager, C. Boge, R. Janissen, D. Rohrbeck, T. Hulsen, S. Lensing-Hohn, R. Krauspe and M. Herten, *Int. J. Periodontics Restor. Dent.*, 2013, **101**, 2905–2914.
30 P. Brun, M. Scorzeto, S. Vassanelli, I. Castagliuolo, G. Palu, F. Ghezzo, G. M. Messina, G. Iucci, V. Battaglia, S. Sivolella, A. Bagno, G. Polzonetti, G. Marletta and M. Dettin, *Acta Biomater.*, 2013, **9**, 6105–6115.
31 H. Lee, S. M. Dellatore, W. M. Miller and P. B. Messersmith, *Science*, 2007, **318**, 426–430.
32 Y. H. Ding, M. Floren and W. Tan, *Biosurf. Biotribol.*, 2016, **2**, 121–136.
33 Y. Liu, K. Ai and L. Lu, *Chem. Rev.*, 2014, **114**, 5057–5115.
34 M. Liu, J. Zhou, Y. Yang, M. Zheng, J. Yang and J. Tan, *Colloids Surf., B*, 2015, **136**, 74–83.
35 S. H. Ku, J. Ryu, S. K. Hong, H. Lee and C. B. Park, *Biomaterials*, 2010, **31**, 2535–2541.
36 C. Y. Chien and W. B. Tsai, *ACS Appl. Mater. Interfaces*, 2013, **5**, 6975–6983.
37 C. Y. Chien, T. Y. Liu, W. H. Kuo, M. J. Wang and W. B. Tsai, *Int. J. Periodontics Restor. Dent.*, 2013, **101**, 740–747.
38 K. Mustafa, A. Oden, A. Wennerberg, K. Hultenby and K. Arvidson, *Biomaterials*, 2005, **26**, 373–381.
39 B. Chehroudi, T. R. Gould and D. M. Brunette, *J. Biomed. Mater. Res.*, 1990, **24**, 1203–1219.
40 M. Quirynen, M. Marechal, H. J. Busscher, A. H. Weerkamp, P. L. Darius and D. van Steenberghe, *J. Clin. Periodontol.*, 1990, **17**, 138–144.
41 P. Gehrke, A. Tabellion and C. Fischer, *J. Adv. Prosthodont.*, 2015, **7**, 151–159.
42 F. R. Kloss, D. Steinmuller-Nethl, R. G. Stigler, T. Ennemoser, M. Rasse and O. Hachl, *Clin. Oral Implants Res.*, 2011, **22**, 699–705.
43 D. Choquet, D. P. Felsenfeld and M. P. Sheetz, *Cell*, 1997, **88**, 39–48.
44 U. Hersel, C. Dahmen and H. Kessler, *Biomaterials*, 2003, **24**, 4385–4415.
45 P. M. Bartold, L. J. Walsh and A. S. Narayanan, *Periodontology*, 2000, **24**, 28–55.
46 R. G. LeBaron and K. A. Athanasiou, *Tissue Eng.*, 2000, **6**, 85–103.
47 E. Ruoslahti, *Annu. Rev. Cell Dev. Biol.*, 1996, **12**, 697–715.
48 S. Yamano, A. K. Ma, R. M. Shanti, S. W. Kim, K. Wada and C. Sukotjo, *Int. J. Oral Maxillofac. Implants*, 2011, **26**, 1247–1255.
49 J. Takagi, *Biochem. Soc. Trans.*, 2004, **32**, 403–406.
50 N. Faucheux, R. Schweiss, K. Lutzow, C. Werner and T. Groth, *Biomaterials*, 2004, **25**, 2721–2730.
51 W. T. Chen and S. J. Singer, *J. Cell Biol.*, 1982, **95**, 205–222.
52 D. S. Wong, J. Li, X. Yan, B. Wang, R. Li, L. Zhang and L. Bian, *Nano Lett.*, 2017, **17**, 1685–1695.
53 V. Rutkunas, V. Bukelskiene, V. Sabaliauskas, E. Balciunas, M. Malinauskas and D. Baltriukiene, *J. Mater. Sci. Mater. Med.*, 2015, **26**, 169.
54 J. D. Humphries, P. Wang, C. Streuli, B. Geiger, M. J. Humphries and C. Ballestrem, *J. Cell Biol.*, 2007, **179**, 1043–1057.
55 A. A. Palaiologou, R. A. Yukna, R. Moses and T. E. Lallier, *J. Periodontol.*, 2001, **72**, 798–807.
56 Y. Qian, X. Zhao, Q. Han, W. Chen, H. Li and W. Yuan, *Nat. Commun.*, 2018, **9**, 323.
57 S. J. Bogdanowich-Knipp, S. Chakrabarti, T. D. Williams, R. K. Dillman and T. J. Siahaan, *J. Pept. Res.*, 1999, **53**, 530–541.
58 M. Kato and M. Mrksich, *Biochemistry*, 2004, **43**, 2699–2707.
59 S. Wohlrab, S. Muller, A. Schmidt, S. Neubauer, H. Kessler, A. Leal-Egana and T. Scheibel, *Biomaterials*, 2012, **33**, 6650–6659.
60 S. P. Massia and J. Stark, *J. Biomed. Mater. Res.*, 2001, **56**, 390–399.

61 B. T. Houseman and M. Mrksich, *Biomaterials*, 2001, **22**, 943–955.
62 M. C. Cortizo, T. G. Oberti, M. S. Cortizo, A. M. Cortizo and M. A. Fernandez Lorenzo de Mele, *J. Dent.*, 2012, **40**, 329–337.
63 Z. Cai, Y. Li, Y. Wang, S. Chen, S. Jiang, H. Ge, L. Lei and X. Huang, *Photochem. Photobiol.*, 2019, **95**, 839–845.
64 R. Xing, I. L. Witso, D. Jugowiec, H. Tiainen, M. Shabestari, S. P. Lyngstadaas, J. Lonn-Stensrud and H. J. Haugen, *Biomed. Mater.*, 2015, **10**, 055003.
65 T. G. van Kooten, J. M. Schakenraad, H. C. van der Mei and H. J. Busscher, *Biomaterials*, 1992, **13**, 897–904.
66 V. E. Wagner and J. D. Bryers, *Int. J. Periodontics Restor. Dent.*, 2004, **69**, 79–90.
67 P. H. Chua, K. G. Neoh, E. T. Kang and W. Wang, *Biomaterials*, 2008, **29**, 1412–1421.
68 T. He, Z. L. Shi, N. Fang, K. G. Neoh, E. T. Kang and V. Chan, *Biomaterials*, 2009, **30**, 317–326.
69 L. G. Harris, S. Tosatti, M. Wieland, M. Textor and R. G. Richards, *Biomaterials*, 2004, **25**, 4135–4148.
70 J. Buxadera-Palomero, C. Calvo, S. Torrent-Camarero, F. J. Gil, C. Mas-Moruno, C. Canal and D. Rodriguez, *Colloids Surf., B*, 2017, **152**, 367–375.
71 L. Su, Y. Yu, Y. Zhao, F. Liang and X. Zhang, *Sci. Rep.*, 2016, **6**, 24420.

